Characterisation of Surrogate Ribs with Variation of the Anterior-Posterior Load Angle: A New Test Methodology.

Marcin Jenerowicz, Florian Kölble, Matthias Boljen, Stefan Hiermaier

Abstract In this study, an innovative setup was employed to test rib surrogates using a drop tower with an adaptable carriage guidance system at dynamic loads up to 1500 mm/s. A new rib model was created using fused filament fabrication (FFF) with P-PLA™ material, aiming to investigate failure mechanisms under varying test angles and comparing them to specific, male post-mortem human subjects (PMHS) data from the literature. The primary objective was to understand fracture dynamics resulting from different load orientation and filament printing directions. Horizontal printing increased fracture resistance, while vertical printing facilitated better control over internal supports, achieving desired fracture behaviour. The experiments involved varying the force application angle (αPH), demonstrating its significant impact on deformation and strain distribution within the specimens. Results included detailed analysis of force-time curves and strain distribution using 3D digital image correlation (3D-DIC). The study emphasises the importance of refining methods, materials, and test setups to improve the validation and applicability of surrogate models. Future research will focus on optimising test conditions and expanding surrogate variations to better capture a broad range of human biomechanical responses, contributing to enhanced accuracy and reliability in ballistic PPE assessments.

Keywords Additive manufacturing, Digital image correlation, High dynamic drop test, PMHS data, Rib bone surrogates.

I. INTRODUCTION

The development of personal protective equipment (PPE) for ballistic applications requires an understanding of the human body's response to high dynamic loads from back face deformation (BFD). Body armour absorbs kinetic energy from projectiles, reducing severe impacts [1]. High dynamic loads can cause contusions, tissue ruptures, fractures, and cardiac injuries, depending on the impact point [2–3]. Understanding these effects is crucial for PPE development.

The US Department of Justice sets a maximum BFD of 44 mm using Roma Plastilina No. 1 to evaluate armour effectiveness [4]. While this serves as a standard for PPE efficiency, it has limitations, such as not correlating with specific injury levels and offering only a 'pass/fail' classification. The impression depth in clay lacks additional injury information. Although the model was deemed species-independent, it was validated only on goat studies [5]. Experts suggest studying larger animals to ensure applicability to humans [6].

Advancements in PPE development focus on improving reliability and comparability, including using anthropomorphic test devices (ATDs). Originating in the automotive industry, ATDs are used in standardised crash tests with predefined scenarios, making them suitable for similar test configurations [7–8]. Due to their automotive origins, most ATDs are unsuitable for ballistic applications [9]. Consequently, new anthropomorphic human surrogate models for ballistic injury assessment have been developed. These include AUSMAN, a reusable mechanical surrogate by the Australian Department of Defense [10]; HSTM, Human Surrogate Torso Model [11]; BTTR, Blunt Trauma Torso Rig [12]; MHS, Modular Human Surrogate [13]; SSO, Skin Skeleton Organs [14]; and SurHUByx, Surrogate Hermaphrodite Universal Body YX [15]. The AUSMAN was compared to experimental post-mortem human subject (PMHS) data during development to validate the effects of chest impact based on the risk of sternal fracture. The HSTM, SSO and MHS were not compared with PMHS data. These assume that the use of

M. Jenerowicz (e–mail: marcin.jenerowicz@emi.fraunhofer.de; tel: +49–761–2714–359) is a Research Fellow at the Fraunhofer Institute for High–Speed Dynamics, Ernst–Mach–Institute (EMI), and a PhD candidate at the Faculty of Engineering of the Albert–Ludwigs–University in Freiburg, Germany. S. Hiermaier is Professor for Sustainable Systems Engineering at the Faculty of Engineering of the Albert–Ludwigs–University and the Director of the Fraunhofer Institute for High–Speed Dynamics, EMI. F. Kölble and M. Boljen are affiliated with the Fraunhofer Institute for High–Speed Dynamics, EMI, Germany.

surrogate materials with comparable characteristic values to human tissue will lead to similar dynamic behaviour. However, there is no definite verification. The SurHUByx model was validated using experimental PMHS data in connection with a ballistic impact. The main shortcoming of these models is the validation of the separate components, e.g. ribs, under given dynamic boundary conditions from PMHS tests. This study presents a method to close this gap.

Rib cortical bone properties change with age [16–18]. However, structural properties are influenced by factors like sex, body size, BMI, cortical thickness [16][18–23], and strain rate dependence of compact bone tissue [24–25]. Although several studies have focused on local rib characterisation [22][26–31], these are confined to specific areas and do not accurately depict every point of the rib cage. The challenge in rib geometry characterisation is differentiating thin and irregular zones and representing the complex structure of trabecular and cortical bone. Mayeur's study [19] employed techniques like multi-scale imaging to analyse local measures such as cross-sectional areas, cortical and trabecular bone percentages, moment of inertia, and variations in cortical thickness across different locations. Material properties and parameters for all ribs throughout the rib arch length of 18 PMHS in rib levels 1 to 10 were documented [19].

The aim of the current study is to examine previously developed and tested rib surrogates [32–33], using a new test methodology. All test devices with an anterior-posterior load are based on Charpail's design [27]. The load application via an impact pendulum can initiate a deformation speed of up to 2000 mm/s, which is derived from the deformation of the rib cage in a frontal impact. Higher test speeds cannot be realised. For this purpose, a new test setup was integrated into a drop tower, which allows for testing at significantly higher test velocities. This also provides the possibility of analysing strain rate dependencies. The natural bilateral curvature of ribs makes it difficult to align the test specimens. The orthogonal alignment of the specimen ends results in an unnatural curvature of the rib arch. In his work [31], Kemper implemented a shift in the lateral x-direction, but the influence of various angles were not investigated in more detail. Hence, a carriage guidance system was integrated that can control the adjustment of the test angle and the application of loads. This opens new possibilities for testing the influence of the angle on the failure mechanisms.

II. METHODS

The following paragraphs outline the surrogate model structure and the configuration of the test equipment.

Model and Material Specifications

The CAD model from the 5th rib surrogate was used from previous studies [32–33]. These studies showed that the predominantly used compound was not sufficiently brittle. Therefore, a new material was used for the present study. The Markforged X3™ utilises fused filament fabrication (FFF) for printing. In FFF, thermoplastic filament is melted and layered onto a platform using an extruder, hardening as it cools. The extrusion process involves software-managed support material, with both main and support structures made from the same material due to a single nozzle. Internal support structures, based on specimen shape, cannot be removed and affect the overall strength and stiffness. External supports, however, can be fully removed. Structure density is influenced by filament width and spacing; this study adheres to standard manufacturer parameters and recommended packing density. The material used is P-PLA™, a polylactic acid whose material properties are summarised in Table I.

TABLE I
MATERIAL PROPERTIES FOR THE P-PLA™ [34]

	Units	Value
Material density	g/cm^3	1.3
Young's modulus	GPa	2.3
Yield strength	MPa	31
Tensile strength at break	MPa	18
Elongation at break	%	27
Flexural strength	MPa	43
Flexural modulus	GPa	2.3

Figure 1 shows the rib surrogate model used in the previous studies [32–33]. Due to the layer thickness and width of the FFF system, all cortical bone thicknesses (Th.e, Th.i, Th.b, Th.t) over the course of the costal arch were extended to 2 mm, which corresponds to approximately four polymer layers of the P-PLA™ material.

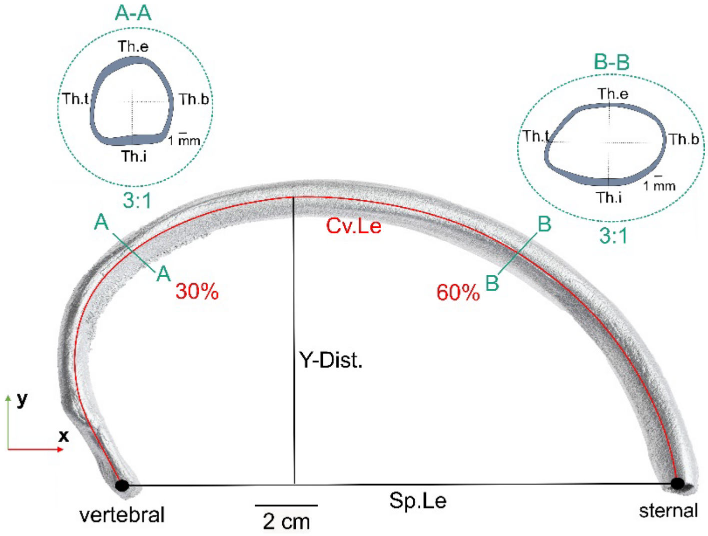

Fig. 1. Fifth rib surrogate from additive manufacturing, including global geometry (Table II), and detailed representation of the cross-sectional areas at 30 % and 60 % Cv.Le with threefold enlargement and corresponding thicknesses of the cutaneous and pleural regions (Th.e, Th.i), and transition zones of the caudal and cranial directions (Th.b, Th.t) [33].

Table II summarises the specific geometric characteristics (Cv.Le: curve length of rib from head to sternal end, Sp.Le: span length from centre of vertebral end to centre of sternal end, y-Dist.: largest distance from x-axis to surface of cutaneous cortex) with comparative values from PMHS data.

TABLE II
GEOMETRIC PROPERTIES OF DEVELOPED RIB SURROGATES AND PARAMETER OF COMPARISON FROM PMHS MALE RIBS

	Cv.Le (mm)	**Sp.Le (mm)**	***y*-Dist. (mm)**
Surrogate	326	177	88
PMHS male 5th rib [27]	N/A	201.0 ± 15.7	N/A
PMHS male 5th rib [31]	317.5 ± 15.9	190.6 ± 14.5	93.6 ± 8.1
PMHS mid-size male 4th-7th rib lv. [30]	303.8 ± 23.4	215.7 ± 19.5	76.4 ± 8.7
PMHS 3th-8th rib lv. [22]	289.4 ± 30.2	204.1 ± 24.0	72.8 ± 9.6

Specimen Configurations

Figure 2 a) shows an overview of the configurations used in the new test setup. By moving the lower carriage, it is possible to vary the angle of force application. This angle corresponds to the pump-handle parameter (αPH) of a rib and is specified as the angle between the local x-axis of the rib and the coronal plane [35], as shown in Figure 2 b). In the original test configuration according to Charpail *et al.* [27], the rib test specimen were aligned orthogonally to the two ends (Fig. 2 a), Config. I, αPH = 90°). If the rib test specimen is aligned planar to its upper arc length, an angle of 90° - αPH = 5° is created (Fig. 2 a), Conf. II). Looking at the human rib cage (male 50 percentile), the αPH corresponds to an average of 50° [35] (Fig. 2 a), Conf. III). These three variations were investigated in the present study. Before testing, the rib surrogates were cast in aluminium square tubes (30 x 30 mm, d = 3 mm) with the polyurethane cast resin Resinpal 1818. To ensure correct alignment of the individual configurations, plastic plates with recesses for the square tubes that predefined the orientation, were used for bonding. This prevents the samples from displacing while curing.

In addition, the influence of the filament printing direction in the FFF system was examined. All test specimens were manufactured in a vertical direction, pointing y-Dist to the printing plane. This enables the control and reduction of the support material used within the specimen. If the specimens are manufactured in the horizontal direction, there are more support structures in the hollow area of the specimen and the paths of the manufacturing process extend over the entire specimen geometry. In order to investigate this influence, the two printing paths were examined in configuration I (specimen description: V - vertical, H - horizontal, O - orthogonal force application corresponds to Conf. I).

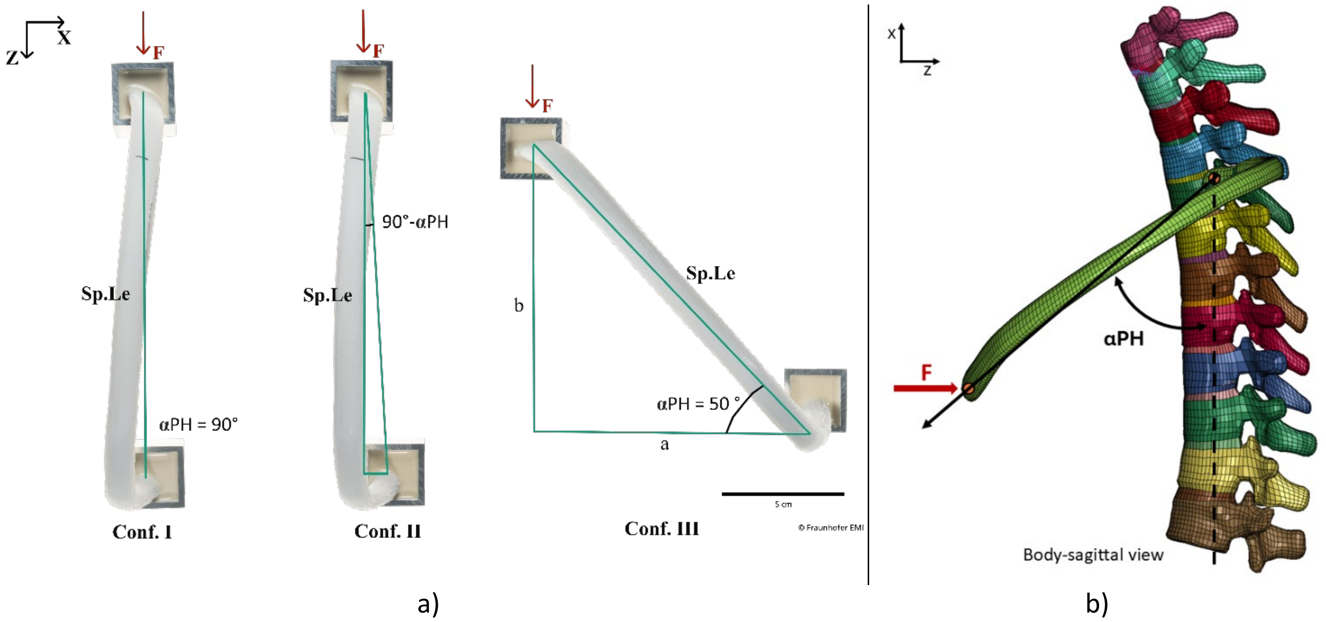

Fig. 2. a) Overview of the test configurations. Conf. I: Orthogonal alignment of the rib at the respective ends (αPH = 90°). Conf. II: Angle change of 90°-αPH = 5° to achieve an orthogonal alignment of the rib arch. Conf. III: Angle change of αPH = 50° to achieve a characteristic force transmission into the costal arch (same position as in a M50 Thorax [35]), $a = 105$ mm, $b = 120$ mm. b) Rib plane parameterization into pump-handle angle (αPH) based on the GHBMC-M50-P thorax model (male 50 percentile) with the left 5th rib.

Table III shows the different experimental conditions with the number of tests carried out.

TABLE III
EXPERIMENTAL CONDITIONS AND NUMBER OF SPECIMEN TESTED

	Conf. I (αPH = 90°)	Conf. II (90°- αPH = 5°)	Conf. III (αPH = 50°)
P-PLA™ V-O	5	5	5
P-PLA™ H-O	5	-	-

Experimental Testing

Figure 3 shows the test setup. The objective was to adapt the original setup according to Charpail *et al.* [27] into a vertical drop tower.

Two carriage systems were installed to define the test direction and to be able to vary the angle of incidence αPH. The drop weight has its own carriage system to which weight plates were attached in order to achieve the required maximum failure load (20 kg). The load is applied directly to the upper slide of the linear guide (sternal end) via a connecting element and has a predefined maximum traversing path of 90 mm, which was derived from previous investigations. For achieving the required velocity, the weight plate was lifted to 200 mm using an electronic crane system. After passing through the drop height, the weight plate is damped by two hydraulic shock absorbers (*ACE* SCS45). The springs of the damper are touched 48.5 mm before the end position of the force plate and are fully retracted at the rear edge. This is to ensure that the vibrations do not propagate too severely to the load cell (*Kistler* 9347B, 5kN). A magnetic band is attached to the upper carriage and in parallel to it, the magnetic sensor (*SIKO* MSC500), which measures the traverse speed directly on the sternal carriage. Both ends of the test specimen are only fixed in the x-direction (Fig. 3) and can rotate freely around the x-axis. An inertial sensor (SICK TMM22) is attached to the back of the specimen holder to monitor the rotation during the test. The displacement and resulting strains were recorded using three-dimensional digital image correlation (3D-

DIC, GOM Correlate Software) with a resolution of 15 pixels/mm. A fine speckle pattern with an approximate speckle size of 0.1 mm was created with an airbrush gun on the anterior (cutaneous) side. The deformation images were taken with high-speed Photron FASTCAM APX-RS cameras with a resolution of 640x 1024 at 4000 fps. By changing the αPH angle in Conf. III, the height of the cameras and resolution was adjusted to 896 x 736.

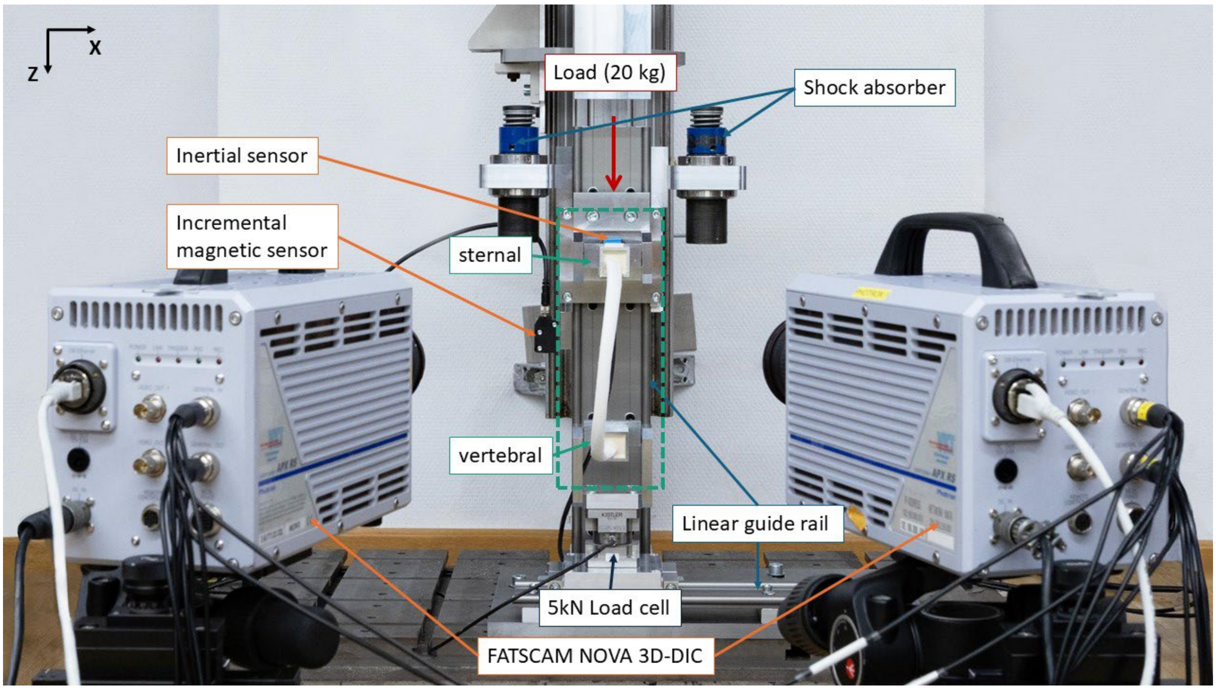

Fig. 3. Experimental setup with surrogate rib in fixture and location of instrumentation, the primary orientation of loading is in Z-direction, where the sternal end is moved toward the vertebral end by the test piston.

III. RESULTS

The PMHS experimental data from literature [22][27][30–31] was used for comparison. Where possible, only data from male 22+ year old subjects and the 5th rib were used to provide a suitable data set for comparison to the surrogates. The following metrics were used: peak force, x-displacement and peak strain @60% Cv.Le at the time of fracture t_{break} (average values of all samples tested).

Five samples were prepared for each test series, whereby sample V-O 04 broke prematurely in the clamping device and was considered invalid. This means that a total of 19 valid tests were carried out. Figure 4 shows an exemplary force-time curve of the tests (specimen V-O 03). The trigger for the cameras is initiated at 50 N (t = 0.0). The initial noise of the curve results from the impact of the weight plate on the fixture and the shock absorbers. This is followed by the deformation phase, which results in the fracture of the specimen at t = 0.043 s. Figure 5 shows the average strains of all specimen configurations, evaluated at 60% Cv.Le. From previous studies, it is known that this is the position with the largest strains [32].

The path of the curve in Fig. 5 corresponds to the force progression in Fig. 4. The initial deformation transitions to the rotational phase until the maximum torsion of the sample around the x-axis is reached, and then increases continuously until fracture. The difference between the two print variations H-O and V-O can also be clearly seen here. The H-O specimens, which were produced horizontally, did not break in any of the tests. Due to the longer application of the filament paths over the entire length of the sample sheet, there is no fracture edge. The specimens buckle at the vertebral end and therefore do not break. This results in significantly higher strains at 60 % Cv.Le at the time of buckling for the H-O specimens. A closer look at the range of the initial torsion (up to t = 0.015 s) shows that there are clear differences between the other vertical specimens. V-O and H-O from Conf. I have a comparable torsional range. Aligning the specimen by 90°- αPH = 5° results in a larger rotation and consequent strains. The adjustment to αPH = 50°, as occurs in the real rib cage, results in a significantly more uniform distribution of strains, which have an almost linear increase up to fracture. Unfortunately, the distribution of the forces in the x and z directions does not allow a direct comparison with PMHS data, as no comparable tests exist to date.

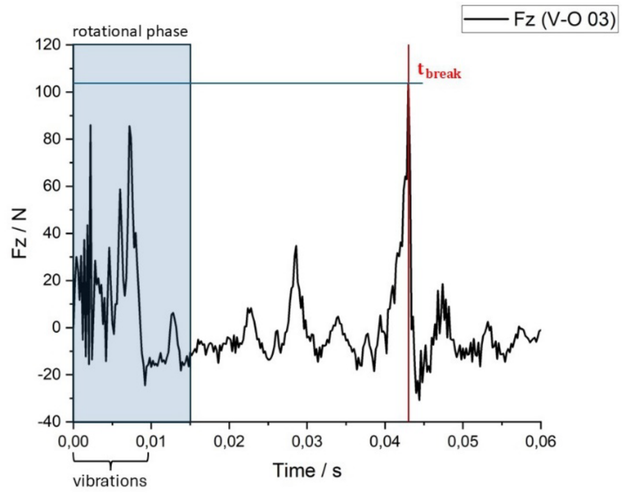

Fig. 4. Characteristic force-time signal of the load cell (exemplary for specimen V-O 03). In the first period (up to 0.01 s) a noise signal can be observed, caused by the first contact of the load cell. This is followed by a decay of the vibrations until the sample breaks at 0.043 s.

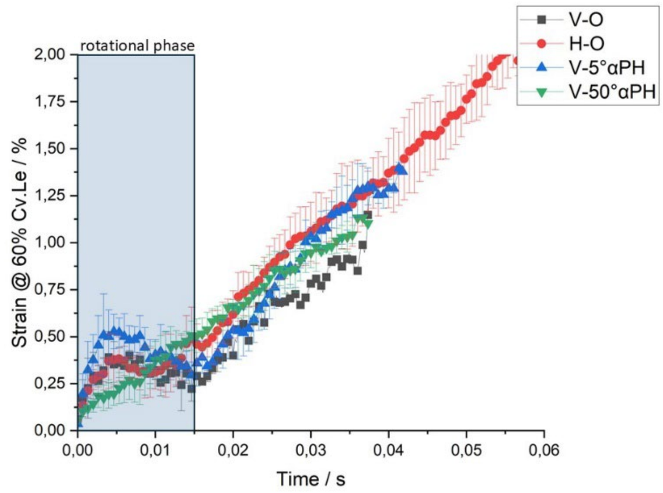

Fig. 5. Strain-time history data of all specimen configurations at 60 % Cv.Le on the cutaneous side at dynamic load rate (1500 mm/s).

All measured characteristic values and the comparison with the PMHS data are summarised in Table IV.

TABLE IV
RESULTS FOR THE STRUCTURAL PROPERTIES WITH STANDARD DEVIATION

Specimen Configuration	$F_{z,max}$ (N)	$F_{x,max}$ (N)	ε_{max} (%)	t_{break} (s)	Test velocity (mm/s)
V-O *(Conf. I)*	123.44±32.36	N/A	1.02±0.06	0.042±0.008	1561±18
H-O *(Conf. I)*	135.60±26.69	N/A	2.16±0.14	0.045±0.003	1502±39
V-5° *(Conf. II)*	169.88±44.03	N/A	1.29±0.09	0.046±0.003	1535±60
V-50° *(Conf. III)*	55.16±5.51	54.56±11.98	1.09±0.12	0.049±0.004	1533±61
PMHS male 5th rib [27]	98.3 ± 36.9	N/A	1.11 ± 0.19	N/A	~1750
PMHS male 5th rib [31]	82.5 ± 18.3	N/A	1.02 ± 0.18	N/A	~1000
PMHS mid-size male 4th-7th rib lv. [30]	116.2 ± 46.6	N/A	1.27 ± 0.66	N/A	~2000
PMHS 3th-8th rib lv. [22]	114.6 ± 41.4	N/A	N/A	N/A	~2000

IV. DISCUSSION

The presented method for the experimental testing of rib surrogates with the variation of the angle of incidence αPH is a unique approach. It could be shown that the angle has an influence on the propagation of the occurring maximum strains and the deformation of the specimen. The vibrations observed in the force-time curve could be minimised by using supplementary shock absorbers and decoupling the mount from the specimen slide. Nevertheless, noise can be observed in the force measurement in the range up to 0.01 s. As the fracture of the sample occurs between 0.04-0.05 s, the influence is considered negligible.

The inertial sensor used in the tests was subject to a time delay. The torsion could be measured, but with a significant time offset of 0.5 s. For further test series, the sampling rate will be adjusted and adapted to the force sensor. In addition, the upper slide was not decoupled from the lower slide after the specimen broke, which led to uncontrolled rotation of the broken specimens and further vibration signals at the force sensor. To prevent this, an additional holder and damper will be installed for the next series of samples. The weight and shape of the upper slide and sample holder will also be adjusted, which should lead to a smoother and more controlled fall of the slide onto the lower part, resulting in less vibrations.

The number of samples tested in this study is limited. New samples have already been produced for the next series of tests, which have a greater variation in cross-sectional shape. This should clearly show how the angle variation αPH affects the geometry and fracture failure. The failure mode and fracture position are crucial for a solid validation of the surrogate structures. The fracture area is relevant but not documented in many PMHS studies. In the study by Agnew *et al.* [22], a distribution of fracture positions is given, which implies that most ribs fracture at 50–90 % of the rib arch length (Cv.Le). This results from the increasingly thinner cross-section. The rib surrogates have a similar structure, and successive examination of the cross-sections will be investigated with the newly fabricated specimens.

The present study has already shown that the printing direction and thus the filament orientation has a major influence on the material behaviour. Due to the horizontal orientation of the sample series H-O, the filaments can achieve an elongation at break of up to 5 %. The 2.16±0.14 % measured here only refer to the maximum value determined without fracture. The long filament paths do not create a break edge, and the samples buckle instead of breaking. The vertical orientation of the samples in production (V-O), in contrast, allows a fracture edge to form between the individual layers, resulting in the desired fracture behaviour compared to literature [22].

The specimen series V-O (Conf. I) is a direct comparison to the PMHS data, as the specimens have the same orientation. Here the deviation in the strains (12.5–20.4 %) is lower than in the forces (32.5–35.3 %). This may be due to the fact that the cross-sections in the predetermined breaking range and at the restraints are still too thick. The relationship between deformation and cross-section will be investigated further. The objective is to use the modified specimens to produce the cross-sections of the surrogates in order to ensure that the fracture behaviour and the characteristic values corresponds nearly to the literature and PMHS test. In addition, the maximum strains and fracture forces should not deviate substantially. With a suitable surrogate in the H-O configuration, successive αPH variations can then be investigated, e.g. corresponding to the change of αPH with increasing age [35].

V. CONCLUSION

In this study, an innovative experimental setup including a drop tower equipped with an adaptable carriage guidance system was used. The experiments included the use of a newly developed rib substitute model printed using a FFF system with P-PLA™ material to investigate the failure mechanisms under variable test angles. The focus was on understanding the fracture dynamics caused by different orientation of the load applied and two different filament directions due to the FFF fabrication process. While horizontal printing of the filaments increases the resistance of the samples to fracture, vertical printing allows better control over the internal supports and leads to the intended fracture behaviour.

The experimental results, which included force-time curves and strain analysis, showed the importance of the force application angle αPH for the deformation and strain distribution in the specimen. However, challenges related to vibration and sensor accuracy emerged, necessitating future adaptations such as improving the specimen bracket and shock absorption to mitigate these issues.

In conclusion, the practical implication of the angle of incidence αPH in the study lies in the influence on the propagation of maximum strains and the deformation of the specimens. Varying this angle allows to better understand the effects on fracture behaviour and geometry, which is crucial for validating surrogate structures. This is essential for designing surrogate models that accurately mimic PMHS rib fracture patterns, thereby improving the accuracy and reliability of assessments capabilities. The study highlights the need for continued refinement of methods, materials, and test setups to enhance the validation and applicability of surrogate models. Future research will focus on optimizing test conditions and expanding surrogate variations to account for a broader range of human biomechanical responses, ensuring that the fracture behaviour aligns closely with literature and PMHS tests. Additionally, investigating αPH variations, corresponding to the change with increasing age, could further enhance the study's viable applications.

VI. ACKNOWLEDGEMENTS

We would like to express our appreciation to the Federal Office of Bundeswehr Equipment, Information Technology and in-Service Support (BAAINBw, Koblenz, Germany), to the Bundeswehr Technical Center for Weapons and Ammunition (WTD–91 GF–450, Meppen, Germany) and to the Bundeswehr Defense Technology Center for Protection and Special Technology (WTD–52 GF–320, Oberjettenberg, Germany) for funding this work.

VII. REFERENCES

[1] Cunniff, P. M. (1996) A Semiempirical Model for the Ballistic Impact Performance of Textile-Based Personnel Armor. Textile Research Journal, **66**(1): pp.45–58.

[2] Lidén, E., Berlin, R., Janzon, B., Schantz, B., Seeman, T. (1988) Some observations relating to behind-body armour blunt trauma effects caused by ballistic impact. The Journal of trauma, **28**(1): pp.S145-8.

[3] Mahajna, A. Aboud, N. *et al*. (2002) Blunt and penetrating injuries caused by rubber bullets during the Israeli-Arab conflict in October, 2000: a retrospective study. Lancet (London, England), 9320: pp.1795–1800.

[4] Ballistic Resistance of Body Armor - NIJ Standard-0101.06 (2008), https://nij.ojp.gov/library/publications/ballistic-resistance-body-armor-nij-standard-010106. [21.03.2023].

[5] Montanarelli, N., Hawkins, C. E., Goldfarb, M. A., Ciurej, T. F. (1973) Defense Technical Information Center, *Protective Garments for Public Officials*, Fort Belvoir, VA.

[6] Hanlon, E., Gillich, P. (2012) Origin of the 44-mm behind-armor blunt trauma standard. Military medicine, **177**(3): pp.333–339.

[7] White, R. P., Rangarajan, N., Haffner, M. (1996) Development of the THOR Advanced Frontal Crash Test Dummy. *Proceedings of the SAFE Conference*, Reno, NV.

[8] Rangarajan, N. Shams, T. *et al.* (1998) Design criteria, design, and performance of the THOR advanced frontal crash test dummy thorax and abdomen assemblies. *Proceedings of the 16th international technical conference on the enhanced safety of vehicles (ESV)*, Ontario, Canada.

[9] Thota, N. M., Epaarachchi, J. A., Lau, K. T. (2014) Review of anthropomorphic test dummies for the evaluation of thoracic trauma due to blunt ballistic impacts. *8th Australasian Congress on Applied Mechanics, ACAM*, Melbourne, Australia.

[10] Bass, C. R. Salzar, R. S. *et al.* (2006) Injury risk in behind armor blunt thoracic trauma. International journal of occupational safety and ergonomics : JOSE, **12**(4): pp.429–442.

[11] Biermann P.J., Ward, E. E., Cain, R. P., Carkhuff, B., Merkle, A. C., Roberts, J. C. (2006) Development of a physical human surrogate torso model for ballistic impact and blast. Advanced Materials, **38**(1): pp.3–12.

[12] Bolduc, M. Anctil, B. (2010) Improved test methods for better protection, a BABT protocol proposal for STANAG 2920. *Proceedings of the Personal Armour Systems Symposium (PASS)*, Quebec City, QC.

[13] Sedberry, K., Foley, S. (2024) Modular human surrogate for non-lethal weapons (NLW) testing. *Technical Report, Defence Systems Information Analysis Center (DSIAC)*.

[14] Yan, W., Yao, X., Wang, Y., Jin, Y., Wei, W. (2020) Experimental study of the mechanical response of a physical human surrogate thoracic model impacted by a rubber ball. Journal of Physics: Conference Series, **1507**(10): pp.102032.

[15] Chaufer, M., Delille, R. *et al*. (2023) A new biomechanical FE model for blunt thoracic impact. Frontiers in Bioengineering and Biotechnology, **11**: pp.1152508.

[16] Kemper, A. R., McNally, C. *et al.* (2005) Material properties of human rib cortical bone from dynamic tension coupon testing. Stapp car crash journal, **49**: pp.199–230.

[17] Stitzel, J. D. Kilgo, P. D., Weaver, A. A., Martin, R. S., Loftis, K. L., Meredith, J. W. (2010) Age thresholds for increased mortality of predominant crash induced thoracic injuries. Association for the Advancement of Automotive Medicine. Annual Scientific Conference, Las Vegas, NV, **54**: pp.41.

[18] Katzenberger, M. J., Albert, D. L., Agnew, A. M., Kemper, A. R. (2020) Effects of sex, age, and two loading rates on the tensile material properties of human rib cortical bone. Journal of the mechanical behavior of biomedical materials, **102**: pp.103410.

[19] Mayeur, O., Chaari, F., Delille, R., Drazetic, P., Markiewicz, E. (2012) Analysis of the cortical bone thickness of human thorax based on multi-scale imaging techniques. Computer methods in biomechanics and biomedical engineering, **15**(1): pp.279–280.

[20] Kalra, A. Saif, T. *et al.* (2015) Characterization of Human Rib Biomechanical Responses due to Three-Point Bending. Stapp car crash journal, **59**: pp.113–130.

[21] Agnew, A., Murach, M., Misicka, E., Moorhouse, K., Bolte IV, J., Kang, Y-S. (2017) The Effect of Body Size on Adult Human Rib Structural Properties. Proceedings of the International Research Council on Biomechanics of Injury: pp.728–736.

[22] Agnew, A. M., Murach, M. M. *et al.* (2018) Sources of Variability in Structural Bending Response of Pediatric and Adult Human Ribs in Dynamic Frontal Impacts. Stapp car crash journal, **62**: pp.119–192.

[23] Velázquez-Ameijide, J., García-Vilana, S. *et al.* (2021) Influence of anthopometric variables on the mechanical properties of human rib cortical bone. Biomedical physics & engineering express, **7**3.

[24] Knets, I., Melnis, A., Dobelis, M. (1999) Effect of Time Dependence on the Mechanical Behavior of Compact Bone Tissue. *IUTAM Symposium on Synthesis in Bio Solid Mechanics*, Copenhagen, Denmark.

[25] Hansen, U., Zioupos, P., Simpson, R., Currey, J. D., Hynd, D. (2008) The effect of strain rate on the mechanical properties of human cortical bone. Journal of biomechanical engineering, **130**(1): pp.11011.

[26] Roberts, S. B., Chen, P. H. (1972) Global geometric characteristics of typical human ribs. Journal of biomechanics, **5**(2): pp.191–201.

[27] Charpail, E., Trosseille, X., Petit, P., Laporte, S., Lavaste, F., Vallancien, G. (2005) Characterization of PMHS Ribs: A New Test Methodology. Stapp car crash journal, **49**: pp.183–198.

[28] Charpail, E., Laporte, S., Trosseille, X., Valancien, G., Lavaste, F. (2006) Material and structure characterization of human ribs. Journal of biomechanics, **39**: pp.S155-S156.

[29] Kindig, M., Lau, A. G., Kent, R. W. (2011) Biomechanical response of ribs under quasistatic frontal loading. Traffic Injury Prevention, **12**(4): pp.377–387.

[30] Kang, Y.-S., Kwon, H. J., Stammen, J., Moorhouse, K., Agnew, A. M. (2021) Biomechanical Response Targets of Adult Human Ribs in Frontal Impacts. Annals of biomedical engineering, **49**(2): pp.900–911.

[31] Kindig, M. W. (2009) Tolerance to Failure and Geometric Influences on the Stiffness of Human Ribs Under Anterior-posterior Loading, *Charlottesville, VA: University of Virginia.*

[32] Jenerowicz, M. Haase, T., Linnenberg, M., Hoschke, K., Boljen, M., Hiermaier, S. (2022) Comparison of rib bone surrogates from additive manufacturing, cast material and PMHS data under dynamic loading. *Proceedings of IRCOBI Conference*, 2022, Porto, Portugal.

[33] Jenerowicz, M., Haase, T. *et al*. (2024) Developing Rib Bone Surrogates for High Dynamic Impact Assessment with Additive Manufacturing and Post-mortem Human Subjects (PMHS)-Based Evaluation. Human Factors and Mechanical Engineering for Defense and Safety, **8**(1).

[34] Markforged. Precise PLA - Materialdatasheet, https://web-objects.markforged.com/craft/materials/Precise-PLA-TDS-REV_3.11.22.pdf. [Accessed 3/11/2022].

[35] Holcombe, S. A., Wang, S. C., Grotberg, J. B. (2017) The effect of age and demographics on rib shape. Journal of Anatomy, **231**(2): pp.229–247.